JACS
JOURNAL OF THE AMERICAN CHEMICAL SOCIETY

pubs.acs.org/JACS

Communication

Adsorption of Nitrogen Dioxide in a Redox-Active Vanadium Metal–Organic Framework Material

Xue Han, Yuexian Hong, Yujie Ma, Wanpeng Lu, Jiangnan Li, Longfei Lin, Alena M. Sheveleva, Floriana Tuna, Eric J. L. McInnes, Catherine Dejoie, Junliang Sun,* Sihai Yang,* and Martin Schröder*

Cite This: *J. Am. Chem. Soc.* 2020, 142, 15235–15239

Read Online

ACCESS | Metrics & More | Article Recommendations | Supporting Information

ABSTRACT: Nitrogen dioxide (NO_2) is a toxic air pollutant, and efficient abatement technologies are important to mitigate the many associated health and environmental problems. Here, we report the reactive adsorption of NO_2 in a redox–active metal–organic framework (MOF), MFM-300(V). Adsorption of NO_2 induces the oxidation of V(III) to V(IV) centers in MFM-300(V), and this is accompanied by the reduction of adsorbed NO_2 to NO and the release of water via deprotonation of the framework hydroxyl groups, as confirmed by synchrotron X-ray diffraction and various experimental techniques. The efficient packing of $\{NO_2 \cdot N_2O_4\}_\infty$ chains in the pores of MFM-300(V^{IV}) results in a high isothermal NO_2 uptake of 13.0 mmol g^{-1} at 298 K and 1.0 bar and is retained for multiple adsorption–desorption cycles. This work will inspire the design of redox-active sorbents that exhibit reductive adsorption of NO_2 for the elimination of air pollutants.

Improving air quality is an important global issue. NO_2 remains a key outdoor air pollutant, with road transport being a major cause, particularly in areas with high population.[1] With increasingly stringent emission standards for vehicles being issued by the World Health Organization (WHO) and other local environmental agencies,[2] refinements and improvements to the existing selective-catalytic-reduction (SCR) systems are required urgently to deliver closer-to-zero emissions of NO_2. While SCR is based on the reduction of NO_x by ammonia or urea at elevated temperatures in the presence of a precious-metal-based catalyst, physio-sorption of gases in porous materials is a well-established method to remove gaseous species. Activated carbons have been long known to remove toxic gases,[3] but these often suffer from low adsorption capacity of NO_2 and/or rapid structural degradation.[4]

Metal–organic frameworks (MOFs) show great potential for gas adsorption and storage, and this is attributed to their large surface area and pore functionalities.[5] Systems incorporating a redox active metal center are of particular interest in gas separation[6] and catalysis.[7] However, adsorption of NO_2 in MOFs remains largely unexplored,[8] and reported studies are based upon breakthrough experiments using gas streams containing NO_2 at ppm levels. In most of these cases, the MOF and MOF-containing composites undergo irreversible structural degradation on adsorption of NO_2. Infrared spectroscopy has been used to characterize the species that are formed upon contacting the surface with highly reactive NO_2.[9−14] Additionally, MOFs have also been explored as new sensing materials for NO_2 detection with high sensitivity and selectivity.[15] Reversible adsorption isotherms for pure NO_2 have been measured with MOFs in only two cases, namely with MFM-300(Al)[16] and MFM-520(Zn).[17] Both materials are highly structurally robust and remain intact throughout the isothermal measurements.

Here we report the reactive adsorption of NO_2 in a redox-active MOF, MFM-300(V) $[V_2(OH)_2(C_{16}H_6O_8)]$. MFM-300(V) is redox active, and both V^{III} and V^{IV} forms, MFM-300(V^{III}) and MFM-300(V^{IV}), can be obtained as pure phase materials.[18] Oxidation of turquoise MFM-300(V^{III}) leads to conversion of the bridging hydroxyl groups to bridging oxo groups in brown MFM-300(V^{IV}) (Figure 1a,b). The adsorption and binding of CO_2[18] and hydrocarbons[19] exhibit notable differences in these two materials with MFM-300(V^{III}) showing higher adsorption uptakes owing to strong hydrogen bonding between substrate molecules and the bridging hydroxyl group.

We introduced NO_2 gas into MFM-300(V^{III}) and collected a series of high-resolution synchrotron X-ray powder diffraction (SPXRD) data. The first three data sets, noted as rapid scan (**RS**, **RS-1**, **RS-2**; ∼8 min for each scan), were collected immediately after loading of NO_2; the final data set, noted as long scan (**LS**; ∼1.5 h), was collected after adsorption had reached equilibrium, as evidenced by the lack of changes in subsequent SPXRD patterns. Rietveld refinement has allowed the determination of binding domains of adsorbed NO_2 molecules and captured key structural changes of the host framework for these models. In the **RS** model of MFM-300(V)·$(NO_2)_{1.67}$, which represents the kinetically favorable state (Figure 1 c, e), only NO_2 was observed and anchored to the pore interior primarily through the hydrogen bonding interaction with the bridging hydroxyl group of the vanadium

Received: June 13, 2020
Published: July 26, 2020

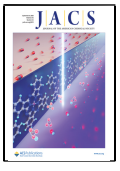

https://dx.doi.org/10.1021/jacs.0c06414
J. Am. Chem. Soc. 2020, 142, 15235–15239

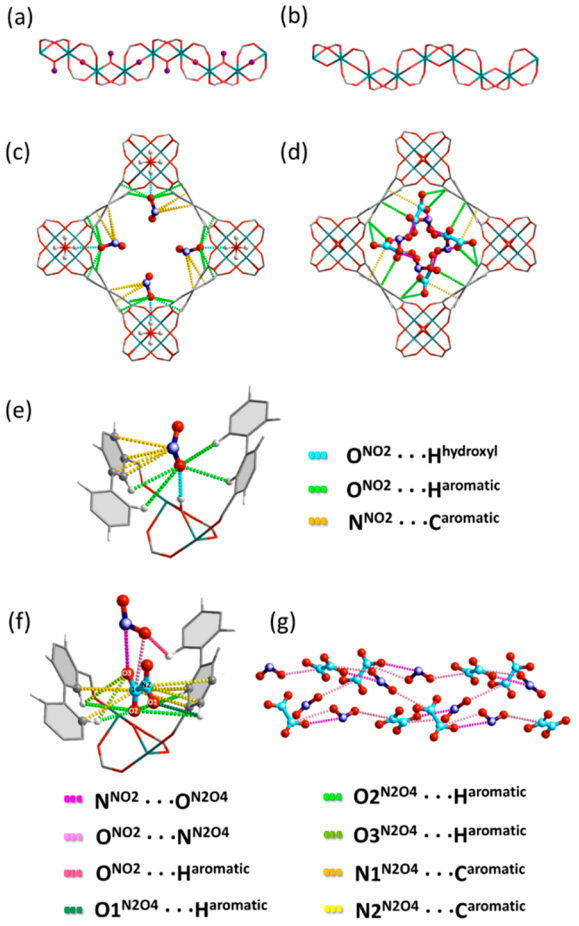

Figure 1. Views along the *a*-axis of the $[VO_6]_\infty$ chain in (a) MFM-300(V^{III}) and (b) MFM-300(V^{IV}) as determined by high-resolution SPXRD data at 298 K. The proton of the bridging hydroxyl group in MFM-300(V^{III}) is highlighted in purple. Views along the *c*-axis of the (c) **RS** and (d) **LS** models showing the packing of guest molecules. Host–guest interactions are enlarged in (e) and (f) for the **RS** and **LS** model, respectively. (g) Extended chain structure of $\{N_2O_4{\cdot}NO_2\}_\infty$ in the **LS** model. V, green; O, red; C, gray; H, white; N of NO_2, deep blue; N of N_2O_4, light blue.

chain [$O^{NO_2}\cdots H^{hydroxyl}$ = 2.33(2) Å]. The bound NO_2 molecule is additionaly stabilized by 8-fold supramolecular interactions with the aromatic ligand of the framework [$O^{NO_2}\cdots H^{aromatic}$ = 3.01(4)–3.59(4) Å; $N^{NO_2}\cdots C^{aromatic}$ = 3.37(2)–3.76(2) Å]. Unlike NO_2@MFM-300(Al),[16] which shows coadsorption and settlement of monomers and dimers of NO_2 (ratio of ~1.0:0.9) in the pores, NO_2@MFM-300(V^{III}) shows only monomers of NO_2 initially with no N_2O_4 dimers in the pores. The framework of MFM-300(V^{III}) [V–O = 1.969(3), 2.005(3), 2.026(4) Å (each appears twice); ∠VO(H)V = 125.6(3)°] is intact in the **RS** model, and bond valence sum (BVS) calcuations confirm an oxidation state of 3.1 for the V center. The structure of **RS-1** [MFM-300(V)·$(NO_2)_{1.66}$] is very similar to that of the **RS** model.

In the **RS-2** model MFM-300(V)·$(NO_2)_{1.28}$·$(N_2O_4)_{1.23}$, we observed an increase of the oxidation state of the vanadium centers and dimerization of NO_2 molecules in the pore; the overall structure is similar to that of the equilibriated **LS** model, which is described now in detail. Upon reaching equilibrium for adsorption of NO_2 in the **LS** model for MFM-300(V)·$(NO_2)_{1.60}$·$(N_2O_4)_{1.53}$, the coordination environment of the V center changes [V–O = 1.831(1), 1.991(2), 2.056(3)Å (each appears twice); ∠VOV = 136.2(1)°], and BVS calculations confirm the increase of valence of the V centers to 3.7 (Figure 1d). Thus, host–guest charge transfer has occurred via the hydrogen bonds of bridging vanadium hydroxyls, which are deprotonated to bridging oxo groups to accommodate oxidation of the V centers in the **LS** model. This has been confirmed further by the disappearance of the –OH stretching band at 3627 cm^{-1} in the FTIR spectrum of the MFM-300(V) on adsorption of NO_2 (Figure 2e). The change

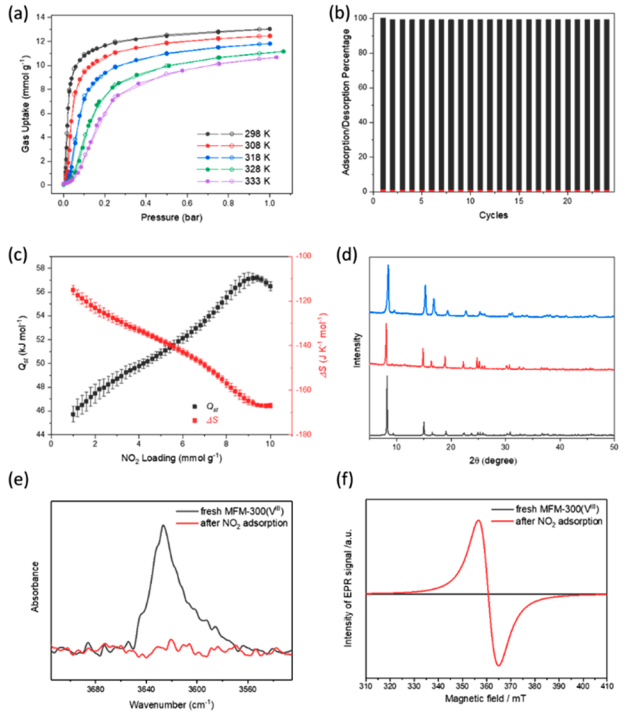

Figure 2. (a) Isotherms for NO_2 uptake in MFM-300(V^{IV}) at 298–333 K (adsorption and desorption are marked with solid and open symbols, respectively). (b) Cyclic adsorption–desorption of NO_2 in MFM-300(V^{IV}) at 298 K between 0 and 0.5 bar. Red bars show the residual NO_2 in the MOF on pressure-swing desorption. (c) Variation of Q_{st} and ΔS for NO_2 uptake in MFM-300(V^{IV}). (d) PXRD patterns of MFM-300(V): simulated (black), as-synthesized (red), and after adsorption and desorption of NO_2 (blue). Comparison of (e) FTIR spectra and (f) X-band (9.87 GHz) EPR spectra of the freshly activated MFM-300(V^{III}) and same sample after adsorption and desorption of NO_2 at 298 K.

in oxidation state of V in MFM-300(V) has also been confirmed by *in situ* EPR spectroscopy where an intense signal centered at g = 1.955 (9.8743 GHz) with a peak-to-peak line width of ca. 75 G appears on adsorption of NO_2 (Figure 2f), consistent with the formation of d^1 V^{IV} centers.[18] This implies that MFM-300(V^{III}) has undergone redox reaction and the proton of the bridging hydroxyl group is removed upon contacting NO_2, yielding weakly adsorbed NO and H_2O that are readily displaced by further molecules of NO_2. This was confirmed by breakthrough experiments (see below). Interestingly, in contrast to the **RS** model, 66% of adsorbed NO_2 molecules in the **LS** model form N_2O_4 dimers, which are stabilized in the pores of MFM-300(V^{IV}) by intermolecular dipole and supramolecular interactions with the aromatic ligands (Figure 1f). This results in a different overall packing of NO_2 and N_2O_4 molecules inside the pores of MFM-300(V^{IV}) compared to that in NO_2@MFM-300(Al).[16] In the **LS** model,

https://dx.doi.org/10.1021/jacs.0c06414
J. Am. Chem. Soc. 2020, 142, 15235–15239

N_2O_4 dimers reside closer to the pore wall while the residual NO_2 monomer is situated more toward the pore center. The host–guest distances [$N^{N_2O_4}\cdots C^{aromatic}$ = 3.34(3)–3.97(2) Å; $O^{N_2O_4}\cdots H^{aromatic}$ = 2.14(4)–3.86(4) Å] are longer in NO_2@MFM-300(V^{IV}) than in NO_2@MFM-300(Al)[16] [3.11(3) Å and 2.62(5)–3.40(5) Å, respectively], indicating an overall weaker host–guest interaction. Alternating dimers and monomers form a 1-D helical chain of $\{N_2O_4{\cdot}NO_2\}_\infty$ running down the pore of the structure along the *c*-axis (Figure 1g). The arrangement of these guest molecules is more compact [$N^{NO_2}\cdots O^{N_2O_4}$ and $O^{NO_2}\cdots N^{N_2O_4}$ distances of 3.10(2)–3.54(3) Å] than in NO_2@MFM-300(Al) [3.33(3)–3.75(3) Å], suggesting that the reduced host–guest interaction in NO_2@MFM-300(V^{IV}) is compensated by the stronger guest–guest interactions to give efficient packing of NO_2.

Gravimetric isotherms for uptake of pure NO_2 in MFM-300(V^{III}) were measured at various temperatures (298–333 K) between 0 and 1.0 bar. All isotherms shown in Figure 2a were measured with the same batch of sample, following the sequence of 298 K, 308 K, 318 K, 328 K, and 333 K. This means that although the sample loaded into the instrument was MFM-300(V^{III}), after initial contact with NO_2 the follow-on isotherms are measuring uptake in MFM-300(V^{IV}), as confirmed by SPXRD results. The NO_2 uptake of MFM-300(V^{IV}) at 298 K and 1.0 bar is 13.0 mmol g^{-1} (equivalent to 2.98 NO_2/V), which is in good agreement with the **LS** model and similar to MFM-300(Al) (14.1 mmol g^{-1} or 2.92 NO_2/Al) under the same conditions. Despite the redox host-to-guest charge transfer, the uptake is fully reversible, and no hysteresis was observed at any temperature. The isothermal uptakes decreased with increasing temperature along the entire pressure range, and the isosteric heats of adsorption (Q_{st}) increase from 46 kJ mol^{-1} steadily to 58 kJ mol^{-1} (Figure 2c), consistent with the presence of strong guest–guest interactions on increased NO_2 loading into MFM-300(V^{IV}). Compared with NO_2@MFM-300(Al),[16] a more negative entropy of adsorption (ΔS) at higher NO_2 loading was observed for MFM-300(V^{IV}), indicating a higher degree of ordering of the N_2O_4/NO_2 molecules in the pore, in excellent agreement with the crystallographic study. The same MFM-300(V^{IV}) sample was then tested across 24 further adsorption–desorption cycles at 298 K, confirming the excellent regeneration of the MOF and no loss of NO_2 uptake (Figure 2b). The crystallinity of MFM-300(V) was retained after all isotherm and cycling measurements (Figure 2d).

Although the initial and the repeated isotherms for NO_2 in MFM-300(V) at 298 K showed equal uptakes at 1.0 bar, when examined more closely, a clear difference of NO_2 uptake can be observed in the low pressure region between these two isotherms. Negligible uptake of NO_2 was recorded in fresh MFM-300(V^{III}) below 10 mbar, whereas once oxidized to MFM-300(V^{IV}) a prominent NO_2 uptake of 1.1 mmol g^{-1} at 10 mbar was observed (Figure S7). We speculated that when NO_2 is contacted with a fresh sample MFM-300(V^{III}), the V center is oxidized and NO_2 is then converted to a poorly adsorbing gaseous species, thus leading to the observed low uptake at low pressures. Whereas for the repeated isotherm at 298 K, MFM-300(V^{IV}) cannot convert further NO_2 and a notable adsorption of 1.1 mmol g^{-1} was observed at 10 mbar. This hypothesis was validated by dynamic breakthrough experiments, where a 900 ppm of NO_2 balanced flow in He was passed through a glass tubular reactor packed with freshly activated MFM-300(V^{III}) at 298 K at a total flow rate of 50 mL min^{-1}. The potential exhaust gaseous products (NO_2, NO, N_2O, N_2, H_2O, CO_2) at the outlet of the fixed-bed were monitored throughout the experiment. After the flow was initiated, a change in the color of the sample from turquoise to brown was clearly observed, starting from the inlet side of the fixed-bed, and this border moved with the gas flow until the entire bed turned brown (Figure 3). This is consistent with the

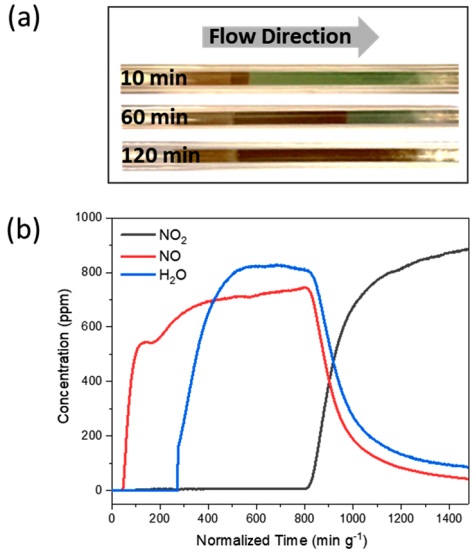

Figure 3. (a) Time-resolved photos of the glass reactor packed with MFM-300(V^{III}) during breakthrough experiment of the NO_2 (900 ppm) in He at 298 K and 1.0 bar showing the color change of sorbent. (b) Breakthrough profiles of species at the outlet of the fixed-bed.

full oxidation of MFM-300(V^{III}) to MFM-300(V^{IV}). Significantly, NO is almost immediately detected after the NO_2 flow was initiated. Thus, upon contact with MFM-300(V^{III}), NO_2 is reduced to NO, which has a much weaker interaction with the framework and is thus readily desorbed and passes rapidly through the fixed bed as confirmed in the dynamic adsorption experiment with NO (Figure S8). This redox reaction is also accompanied by the production of water, which is gradually displaced by molecules of NO_2 and is observed at the outlet after NO owing to its stronger interaction with the framework. Finally, NO_2 is eluted, while the NO concentration returns to near zero, confirming the completion of the redox reaction at MFM-300(V) and the saturation of the fixed-bed by adsorption of NO_2. Throughout the experiment, no other nitrogen-containing species was detected. The breakthrough experiment demonstrates the ability of MFM-300(V) for the dynamic adsorption and reduction of NO_2 even at ppm-level concentrations.

In summary, MFM-300(V^{III}) exhibits redox conversion to MFM-300(V^{IV}) on adsorption of NO_2, which is converted to NO. MFM-300(V^{IV}) shows high capacity and excellent reversibility for NO_2 adsorption suggesting future directions for the development of efficient redox-active sorbent materials to realize adsorptive reduction of NO_2 into nonharmful species.

■ ASSOCIATED CONTENT

Supporting Information

The Supporting Information is available free of charge at https://pubs.acs.org/doi/10.1021/jacs.0c06414.

https://dx.doi.org/10.1021/jacs.0c06414
J. Am. Chem. Soc. 2020, 142, 15235–15239

Synthesis procedures, characterization, and additional analysis of crystal structures and adsorption results (PDF)

Crystal data of MFM-300(V)$(NO_2)_{1.67}$ (CIF)

Crystal data of MFM-300(V)·$(NO_2)_{1.66}$ (CIF)

Crystal data of MFM-300(V)·$(NO_2)_{1.28}$·$(N_2O_4)_{1.23}$ (CIF)

Crystal data of MFM-300(V)·$(NO_2)_{1.60}$·$(N_2O_4)_{1.53}$ (CIF)

AUTHOR INFORMATION

Corresponding Authors

Junliang Sun − *College of Chemistry and Molecular Engineering, Peking University, Beijing 100871, China;* orcid.org/0000-0003-4074-0962; Email: Junliang.Sun@pku.edu.cn

Sihai Yang − *Department of Chemistry, University of Manchester, Manchester M13 9PL, U.K.;* orcid.org/0000-0002-1111-9272; Email: Sihai.Yang@manchester.ac.uk

Martin Schröder − *Department of Chemistry, University of Manchester, Manchester M13 9PL, U.K.;* orcid.org/0000-0001-6992-0700; Email: M.Schroder@manchester.ac.uk

Authors

Xue Han − *Department of Chemistry, University of Manchester, Manchester M13 9PL, U.K.*

Yuexian Hong − *College of Chemistry and Molecular Engineering, Peking University, Beijing 100871, China*

Yujie Ma − *Department of Chemistry, University of Manchester, Manchester M13 9PL, U.K.*

Wanpeng Lu − *Department of Chemistry, University of Manchester, Manchester M13 9PL, U.K.*

Jiangnan Li − *Department of Chemistry, University of Manchester, Manchester M13 9PL, U.K.*

Longfei Lin − *Department of Chemistry, University of Manchester, Manchester M13 9PL, U.K.*

Alena M. Sheveleva − *Department of Chemistry, University of Manchester, Manchester M13 9PL, U.K.*

Floriana Tuna − *Department of Chemistry and Photon Science Institute, University of Manchester, Manchester M13 9PL, U.K.*

Eric J. L. McInnes − *Department of Chemistry, University of Manchester, Manchester M13 9PL, U.K.;* orcid.org/0000-0002-4090-7040

Catherine Dejoie − *European Synchrotron Radiation Facility (ESRF), Grenoble 38043, France*

Complete contact information is available at: https://pubs.acs.org/10.1021/jacs.0c06414

Notes

The authors declare no competing financial interest.

Crystal data of MFM-300(V)$(NO_2)_{1.67}$ and MFM-300(V)·$(NO_2)_{1.60}$·$(N_2O_4)_{1.53}$ are deposited at Cambridge Crystallographic Data Centre (CCDC 1996818−1996819).

ACKNOWLEDGMENTS

We thank EPSRC (EP/I011870), the Royal Society, the National Natural Science Foundation of China, Peking University, and University of Manchester for funding, and EPSRC for funding of the EPSRC National EPR Facility at Manchester. This project has received funding from the European Research Council (ERC) under the European Union's Horizon 2020 research and innovation programme (Grant Agreement No. 742401, *NANOCHEM*). We are grateful to ESRF for access to the Beamline ID22 and thank A. Fitch for the help at ESRF. A.M.S. is supported by a Royal Society Newton International Fellowship. Y.M. and J.L. thank the China Scholarship Council (CSC) and the University of Manchester for funding.

REFERENCES

(1) Ambient (outdoor) air pollution, 2018. World Health Organization Web site. https://www.who.int/news-room/fact-sheets/detail/ambient-(outdoor)-air-quality-and-health (accessed May 2, 2018).

(2) Nitrogen dioxide (NO_2) pollution, 2019. United States Environmental Protection Agency Website. https://www.epa.gov/no2-pollution (accessed June 13, 2019).

(3) (a) Kozhevnikov, A. B. *Stalin's great science: the times and adventures of Soviet physicists*; Imperial College Press: 2004; pp 10−11. (b) Ray, G. C.; Box, E. O. Adsorption of gases on activated charcoal. *Ind. Eng. Chem.* **1950**, *42*, 1315−1318.

(4) (a) Belhachemi, M.; Jeguirim, M.; Limousy, L.; Addoun, F. Comparison of NO_2 removal using date pits activated carbon and modified commercialized activated carbon via different preparation methods: Effect of porosity and surface chemistry. *Chem. Eng. J.* **2014**, *253*, 121−129. (b) Florent, M.; Tocci, M.; Bandosz, T. J. NO_2 adsorption at ambient temperature on urea-modified ordered mesoporous carbon. *Carbon* **2013**, *63*, 283−203.

(5) Li, J. R.; Kuppler, R. J.; Zhou, H.-C. Selective gas adsorption and separation in metal-organic frameworks. *Chem. Soc. Rev.* **2009**, *38*, 1477−1504.

(6) Li, L.; Lin, R. B.; Krishna, R.; Li, H.; Xiang, S.; Wu, H.; Li, J.; Zhou, W.; Chen, B. Ethane/ethylene separation in a metal-organic framework with iron-peroxo sites. *Science* **2018**, *362*, 443−446.

(7) Verma, P.; Vogiatzis, K. D.; Planas, N.; Borycz, J.; Xiao, D. J.; Long, J. R.; Gagliardi, L.; Truhlar, D. G. Mechanism of oxidation of ethane and ethanol at iron(IV)-oxo sites in magnesium-diluted Fe2(dodbc). *J. Am. Chem. Soc.* **2015**, *137*, 5770−5781.

(8) Han, X.; Yang, S.; Schröder, M. Porous metal-organic-framework as emerging sorbents for clean air. *Nat. Rev. Chem.* **2019**, *3*, 108−118.

(9) Levasseur, B.; Petit, C.; Bandosz, T. J. Reactive adsorption of NO_2 on copper-based metal-organic framework and graphite oxide/metal-organic framework composites. *ACS Appl. Mater. Interfaces* **2010**, *2*, 3606−3613.

(10) Petit, C.; Levasseur, B.; Mendoza, B.; Bandosz, T. J. Reactive adsorption of acidic gases on MOF/graphite oxide composites. *Microporous Mesoporous Mater.* **2012**, *154*, 107−112.

(11) Ebrahim, A. M.; Levasseur, B.; Bandosz, T. J. Interactions of NO_2 with Zr-based MOF: effects of the size of organic linkers on NO_2 adsorption at ambient conditions. *Langmuir* **2013**, *29*, 168−174.

(12) Ebrahim, A. M.; Bandosz, T. J. Effect of amine modification on the properties of zirconium-carboxylic acid based materials and their applications as NO_2 adsorbents at ambient conditions. *Microporous Mesoporous Mater.* **2014**, *188*, 149−162.

(13) Peterson, G. W.; Mahle, J. J.; DeCoste, J. B.; Gordon, W. O.; Rossin, J. A. Extraordinary NO_2 removal by the metal-organic framework UiO-66-NH_2. *Angew. Chem., Int. Ed.* **2016**, *55*, 6235−6238.

(14) Ebrahim, A. M.; Bandosz, T. J. Ce(III) Doped Zr-based MOFs as excellent NO_2 adsorbents at ambient conditions. *ACS Appl. Mater. Interfaces* **2013**, *5*, 10565−10573.

(15) Kumar, P.; Kim, K. H.; Rarotra, S.; Ge, L.; Lisak, G. The advanced sensing systems for NOx based on metal-organic frameworks: applications and future opportunities. *Trends Anal. Chem.* **2020**, *122*, 115730.

(16) Han, X.; Godfrey, H. G. W.; Briggs, L.; Davies, A. J.; Cheng, Y.; Daemen, L. L.; Sheveleva, A. M.; Tuna, F.; McInnes, E. J. L.; Sun, J.; Drathen, C.; George, M. G.; Ramirez-Cuesta, A. J.; Thomas, K. M.; Yang, S.; Schröder, M. Reversible adsorption of nitrogen dioxide within a robust porous metal−organic framework. *Nat. Mater.* **2018**, *17*, 691−696.

(17) Li, J.; Han, X.; Zhang, X.; Sheveleva, A. M.; Cheng, Y.; Tuna, F.; McInnes, E. J. L.; McCormick, L. J.; Teat, S. J.; Daemen, L. L.; Ramirez-Cuesta, A. J.; Schröder, M.; Yang, S. Capture of nitrogen dioxide and conversion to nitric acid in a porous metal−organic framework. *Nat. Chem.* **2019**, *11*, 1085−1090.
(18) Lu, Z.; Godfrey, H. G. W.; da Silva, I.; Cheng, Y.; Savage, M.; Tuna, F.; McInnes, E. J. L.; Teat, S. J.; Gagnon, K. J.; Frogley, M. D.; Manuel, P.; Rudić, S.; Ramirez-Cuesta, A. J.; Easun, T. L.; Yang, S.; Schröder, M. Modulating supramolecular binding of carbon dioxide in a redox-active porous metal-organic framework. *Nat. Commun.* **2017**, *8*, 14212.
(19) Lu, Z.; Godfrey, H. G. W.; da Silva, I.; Cheng, Y.; Savage, M.; Manuel, P.; Rudić, S.; Ramirez-Cuesta, A. J.; Yang, S.; Schröder, M. Direct observation of supramolecular binding of light hydrocarbons in vanadium(III) and (IV) metal−organic framework materials. *Chem. Sci.* **2018**, *9*, 3401−3408.

https://dx.doi.org/10.1021/jacs.0c06414
J. Am. Chem. Soc. 2020, 142, 15235−15239